Structural Engineering and Mechanics, *Vol. 52, No. 4 (2014) 787-813*
DOI: http://dx.doi.org/10.12989/sem.2014.52.4.787

Torsional flexural steady state response of monosymmetric thin-walled beams under harmonic loads

Mohammed A. Hjaji[1] and Magdi Mohareb[*2]

[1]*Department of Mechanical and Industrial Engineering, University of Tripoli, Tripoli, Libya*
[2]*Civil Engineering Department, University of Ottawa, 161 Louis Pasteur (A-025), Ottawa, Ontario, K1N 6N5, Canada*

(Received March 26, 2013, Revised July 9, 2014, Accepted July 13, 2014)

Abstract. Starting with Hamilton's variational principle, the governing field equations for the steady state response of thin-walled beams under harmonic forces are derived. The formulation captures shear deformation effects due to bending and warping, translational and rotary inertia effects and as well as torsional flexural coupling effects due to the cross section mono-symmetry. The equations of motion consist of four coupled differential equations in the unknown displacement field variables. A general closed form solution is then developed for the coupled system of equations. The solution is subsequently used to develop a family of shape functions which exactly satisfy the homogeneous form of the governing field equations. A super-convergent finite element is then formulated based on the exact shape functions. Key features of the element developed include its ability to (a) isolate the steady state response component of the response to make the solution amenable to fatigue design, (b) capture coupling effects arising as a result of section mono-symmetry, (c) eliminate spatial discretization arising in commonly used finite elements, (d) avoiding shear locking phenomena, and (e) eliminate the need for time discretization. The results based on the present solution are found to be in excellent agreement with those based on finite element solutions at a small fraction of the computational and modelling cost involved.

Keywords: torsional-flexural response; monosymmetric section; harmonic forces; exact shape functions

1. Introduction

Thin-walled structural members are used as stiffeners in aircraft structures, propellant and turbine blades, steel structures, ships, marine structures and vehicle axles. In these applications, they are commonly subjected to harmonic loading. Sources of harmonic loads include aerodynamics forces, hydro-dynamic wave motion and forces arising from unbalance in rotating machinery, propellants and reciprocating machines. In such applications, thin-walled members are prone to fatigue failures. Under harmonic forces, member response has two components; (1) a transient component which is induced at the beginning of the excitation, and (2) a steady state component which is sustained for a long time. The transient response attenuates quickly due to damping and is thus of no importance for fatigue design. In contrast, the sustained steady state

∗Corresponding author, Professor, E-mail: mmohareb@uottawa.ca

http://www.techno-press.org/?journal=sem&subpage=8 ISSN: 1225-4568 (Print), 1598-6217 (Online)

component of the response is of key for fatigue design, and is the prime focus of the present study.

Thus, the present study aims at developing an efficient solution which isolates the steady state response of thin-walled beams when subjected to harmonic forces. For doubly-symmetric cross-sections, the longitudinal, transverse, lateral response is fully uncoupled from the lateral response. The associated solutions are provided in (Hjaji and Mohareb 2011a, b) under a shear deformable thin-walled beam theory and in (Hjaji and Mohareb 2013a, b) under a shear non-deformable theory. In contrast, for beams with mono-symmetric cross-sections (e.g., I-section with unequal flanges, channel section), the flexural response in the direction normal to the axis of symmetry is observed to be coupled with the torsional response. Under the conventional Vlasov theory (Hjaji and Mohareb 2014a, b), the coupling involves two displacement fields while under the shear deformable theory in the present study, the coupling involves four displacement fields. The challenges associated with formulating a closed form solution of the four-field coupled system are the focus of the present work. The closed form solution is subsequently exploited to develop an efficient finite element for the analysis of beams of mono-symmetric sections under harmonic forces.

2. Literature review

Methods of analysis of thin walled beams under dynamic loads consist of analytical solutions and summarized in Section 2.1 and those based on finite element analysis as summarized in Section 2.2.

2.1 Literature review on analytical solutions

The classical thin-walled beam theory developed by Vlasov (1961) assumes that the beam cross-section does not deform in its own plane, and the transverse shear strains at the middle surface are negligible. The theory has been extensively used in dynamic analysis of thin-walled beams as exemplified by the studies of Friberg (1985), Bishop *et al*. (1989), Leung (1991), Chen and Tamma (1994), Banerjee *et al*. (1996), Li *et al*. (2004a), Kim *et al*. (2007). Bishop and Price (1985) studied the free vibration of thin-walled members with channel-shaped sections. More advanced theories capturing shear deformation effects were also developed by several authors. This includes the work of Dokumaci (1987) who studied the coupled flexural–torsional vibration of thin-walled beams whose study captured warping effects. Tanaka and Bercin (1997) studied the coupled flexural-torsional free vibrations of thin-walled open members. Their solution captured rotatory inertia effects. Using the dynamic transfer matrix method, and the mode superposition technique, Li *et al*. (2004a) formulated a solution for determining the coupled bending-torsion response of thin-walled beams under external random excitations. Their solution accounts for warping and rotary inertia. In a subsequent study, Li *et al*. (2004b) extended their formulations to include the influence of uniform axial forces. Laudiero and Savoia (1991) studied the flexural-torsional vibrations of thin-walled beams with open and closed cross-sections. Their study accounted for the effect of bending and non-uniform torsion, secondary warping and shear lag effects. Tanaka and Bercin (1998) extended their former work (Tanaka and Bercin 1997) to asymmetric sections. Kollar (2001) developed a theory of free vibration analysis of thin- walled open section composite beams including closed-form solutions for the coupled flexural- torsional natural frequencies for simply-supported beams. Cortinez and Piovan (2001) developed an

analytical solution for the free vibration analysis of composite thin-walled beams of open and closed cross-sections. Kim *et al*. (2003) formulated the exact dynamic and static stiffness matrices for the free vibration and stability analysis of thin-walled beams. Their theory accounts for shear deformation effects due to bending and warping torsion and captures the coupling between both effects. Also, they incorporated the rotary inertia effects and the flexural-torsional coupling effects due to the asymmetry of the cross-sections. In a subsequent study, Kim and Kim (2005) adopted the theory in Kim *et al*. (2003) to develop the dynamic stiffness matrix element for the flexural-torsional free vibration of asymmetric thin-walled beams. By applying the Hellinger-Reissner variational principle, the governing equations of motion were derived for the coupled vibration response of thin-walled beams with asymmetric cross-sections and the force-deformation relations. Using the principle of virtual work, Prokic (2006) derived the differential equations for the coupled vibrations of a general thin-walled beam theory capturing shear deformation effects due to bending based on multiple degrees of freedom to express the warping deformation. Closed-form solution for the natural frequencies was derived for the case of simply supported beams. Vo and Lee (2009b) developed a solution based on a shear deformable beam theory for the study of flexural-torsional buckling and vibration analysis of open thin-walled composite beams. Based on a modified Vlasov theory which accounts for shear deformation, Ambrosini (2004) presented a general theory for the coupled flexural-torsional vibration of thin-walled beams of open cross-sections. De Borbon and Ambrosini (2010) extended the theory of Ambrosini (2004) to incorporate the effect of the axial forces. Guinta *et al*. (2014) developed a unified hierarchical treatment for formulating beam theories including shear deformable effects. Based the Vlasov beam theory, and the lamination theory, Prokic *et al*. (2014) developed a technique for determining geometric and material properties of composite thin-walled beams.

2.2 Literature review on finite element formulations

Most finite elements for the dynamic analysis of thin-walled members are based on two approaches. In the first approach, formulations are based on approximate shape functions such as the work of Tanaka and Bercin (1997), Lee and Kim (2002a, b), Voros (2008, 2009), etc. In the second approach, shape functions are based on the solution of the homogeneous solution of the static equilibrium equations, such as the work of Mei (1970), Chen and Tamma (1994), Hu *et al*. (1996). Finite element formulations which omit shear deformation effects includes the work of Mei (1970), Chen and Tamma (1994), Hu *et al*. (1996), Tanaka and Bercin (1998), Hashemi and Richard (2000a, b), Lee and Kim (2002a, b), Voros (2008, 2009). Based on exact shape functions, Mei (1970) developed a finite element for the coupled free vibration analysis of thin-walled beams which incorporated warping effects. Chen and Tamma (1994) formulated a finite element to study the dynamic coupled vibrations of thin-walled open members with arbitrary cross-sections including the influence of constant transverse loads. Their formulation was based on assumed linear and cubic displacement shape functions in conjunction with an implicit self-starting unconditionally stable integration scheme. Hu *et al*. (1996) studied the coupled bending-torsional dynamic behavior of thin-walled beams of asymmetric cross-sections. The shear deformation and bending-torsional coupling effects due to cross-section non-symmetry were fully incorporated in the solution. Hashemi and Richard (2000a) studied the coupled bending-torsional vibration analysis of thin-walled beams by developing a dynamic finite element. The exact solutions of the governing dynamic equations of equilibrium were obtained and, subsequently, frequency-dependent hyperbolic interpolation functions were adopted to formulate the stiffness and mass

matrices of the structure. Later on, Hashemi and Richard (2000b) extended their work to include the effect of axial force. By using linear and cubic Hermitian shape functions, Lee and Kim (2002a, b) investigated the coupled free vibration of thin-walled composite beams with doubly symmetric and channel-shaped cross-sections. The influence of lateral forces on the coupled bending-torsional free vibration of thin-walled open members was studied by Voros (2008, 2009) who formulated a two-noded beam element with fourteen degrees of freedom. Recently, Vo and Lee (2009a, 2010), Vo *et al*. (2010, 2011) studied the coupled flexural-torsional free vibration of thin-walled open composite beams under constant axial forces and end moments by developing a displacement-based one dimensional finite element model. Finite element formulations including shear deformation effects include the work of Kim and Kim (2005) who formulated an isoparametric element to capture the coupled flexural-torsional free vibration of asymmetric thin-walled shear deformable beams. Recently, Vo and Lee (2009c), Vo *et al*. (2009) extended their previous studies for the coupled flexural-torsional composite members to incorporate the shear deformation effects in a finite element formulation based on one-dimensional shear-deformable finite beam element using linear and cubic Hermite shape functions.

A feature common to the above studies is use of approximate shape functions involving spatial discretization errors, and thus requiring fine meshes to converge to the actual solution. In contrast, the present study avoids discretization errors by formulating shape functions which exactly satisfy the homogeneous form of the dynamic equilibrium equations. Another commonality between the above studies is the fact they focus on extracting the free vibration characteristics including extracting the natural frequencies and mode shapes. In contrast, the present study aims at directly extracting the steady state response without the need for extracting the natural frequencies and mode shapes.

3. Basic assumptions

The formulation is based on the following assumptions:

1. Cross-section is open and mono-symmetric with the x axis taken as the axis of mono-symmetry,
2. Member is assumed prismatic,
3. Deformations are assumed small enough for the material to remain within the elastic range of deformation,
4. Strains and rotations are assumed small,
5. Cross-section is assumed to remain undistorted (rigid) in its own plane in a manner consistent with Vlasov's first assumption (Vlasov 1961),
6. For loading not involving twist, a planar cross-section originally normal to the centriodal axis is assumed to remain plane but not perpendicular to the cross-section after deformation, i.e., the transverse shear deformations of the middle-surface of the cross-section are incorporated in the assumed kinematics (in a manner analogous to the Timoshenko beam theory). The assumption is further generalized to twist/warping deformations (i.e., the shear strains induced by warping at the middle surface are non-zero and are characterized by a generalized displacement function multiplied by the sectorial coordinate).

The assumed kinematics can be conceived as a combination of Vlasov and Timoshenko theories. Similar kinematics were assumed in Laudiero and Savoia (1991), Kim *et al*. (2003), Vo

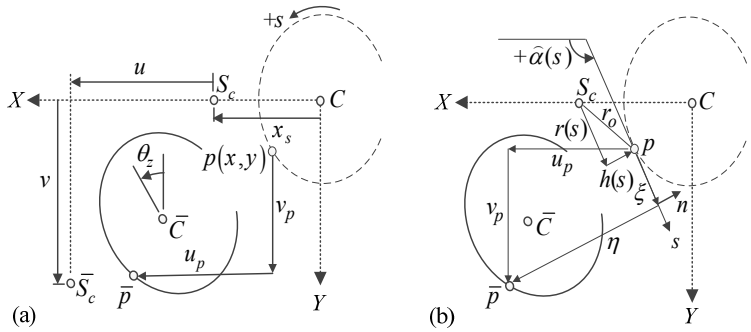

Fig. 1 (a) Local coordinate system and displacement components of a point $p(x,y)$ on the cross-section, (b) tangential and normal displacements

and Lee (2009c), Back and will (1998), Cortinez and Piovan (2001), Li *et al*. (2004c), Machado and Cortinez (2007), Machado (2007), Wu and Mohareb (2011), Librescu and Song (2006).

4. Displacement fields

Based on the above assumptions, the longitudinal displacement $w_p(z,s,t)$ and the in-plane displacements $u_p(z,s,t)$ and $v_p(z,s,t)$ of a general point $p(x(s), y(s))$ located on the mid-surface of the cross-section (Fig. 1) are respectively given by (e.g., Back and Will 1998)

$$w_p(z,s,t)=w(z,t)+y(s)\theta_x(z,t)-x(s)\theta_y(z,t)+\omega(s)\psi(z,t) \tag{1}$$

$$u_p(z,s,t)=u(z,t)-y(s)\theta_z(z,t) \tag{2}$$

$$v_p(z,s,t)=v(z,t)+\left[x(s)-x_s\right]\theta_z(z,t) \tag{3}$$

in which $w(z,t)$ is the average longitudinal displacement along the longitudinal axis z, $u(z,t)$and $v(z,t)$ are the displacement components of the shear centre (x_s, y_s=0) along the principal directions X and Y, $\theta_x(z,t)$ and $\theta_y(z,t)$ are the rotations of the cross-section about X and Y axes, $\theta_z(z,t)$ is the twist angle of the cross-section about the longitudinal axis, $\psi(z,t)$ is a function which characterizes the magnitude of the warping deformation, $\omega(s)$ is the warping function, $x(s)$ and $y(s)$ are the coordinates of a point denoted by a curvilinear coordinates lying on the middle surface of the section and x_s is the coordinate of the shear centre along the axis of symmetry.

The in-plane displacements $u_p(z,s,t)$ and $v_p(z,s,t)$ of the general point p are resolved into tangential and normal displacement components $\xi(z,s,t)$ and $\eta(z,s,t)$ along the tangential t and normal n directions, respectively, (Fig. 1(b)), yielding

$$\xi(z,s,t)=u(z,t)\cos\hat{\alpha}+v(z,t)\sin\hat{\alpha}+h(s)\theta_z(z,t) \tag{4}$$

$$\eta(z,s,t)=v(z,t)\cos\hat{\alpha}-u(z,t)\sin\hat{\alpha}+r(s)\theta_z(z,t) \tag{5}$$

where $h(s)=x(s)\sin\hat{\alpha}-y(s)\cos\hat{\alpha}$, $r(s)=x(s)\cos\hat{\alpha}+y(s)\sin\hat{\alpha}$, $\sin\hat{\alpha}=dy(s)/ds$, $\cos\hat{\alpha}=dx(s)/ds$, $h(s)=d\omega(s)/ds$, and $\hat{\alpha}(s)$ is the angle between the tangent of the cross-section of point p and the X

axis (Fig. 1(b)). The member is assumed to be subjected to general applied harmonic forces within the member

$$\begin{aligned} &q_x(z,t), q_y(z,t), q_z(z,t), m_x(z,t), m_y(z,t), m_z(z,t), m_w(z,t) \\ &\quad = \left[\bar{q}_x(z), \bar{q}_y(z), \bar{q}_z(z), \bar{m}_x(z), \bar{m}_y(z), \bar{m}_z(z)\, \bar{m}_w(z)\right] \mathrm{e}^{i\Omega t} \end{aligned} \tag{6}$$

and the end harmonic forces

$$\begin{aligned} &N_z(z_e,t), V_x(z_e,t), V_y(z_e,t), M_x(z_e,t), M_y(z_e,t), M_z(z_e,t), M_w(z_e,t) \\ &\quad = \left[\bar{N}_z(z_e), \bar{V}_x(z_e), \bar{V}_y(z_e), \bar{M}_x(z_e), \bar{M}_y(z_e), \bar{M}_z(z_e), \bar{M}_w(z_e)\right] \mathrm{e}^{i\Omega t}, \text{ for } z_e = 0, \ell \end{aligned} \tag{7}$$

in which Ω is the circular frequency of the applied loads, $i = \sqrt{-1}$ is the imaginary constant, $q_x(z,t)$, $q_y(z,t)$, $q_z(z,t)$ are distributed harmonic forces, $m_x(z,t)$, $m_y(z,t)$, $m_z(z,t)$ are the distributed harmonic moments, $m_w(z,t)$ is the distributed harmonic bimoment, $N_z(z_e,t)$, $V_x(z_e,t)$, $V_y(z_e,t)$ are the longitudinal, transverse and lateral harmonic forces at member ends z_e=0, ℓ, $M_x(z_e,t)$, $M_y(z_e,t)$, $M_z(z_e,t)$ are harmonic end moments and $M_w(z_e,t)$ are harmonic end bimoments. The applied forces are assumed to have the same sign convention as those of the end displacement components (Fig. 1(a)). Under the above applied harmonic forces, the steady state component of the response is assumed to take the form

$$\begin{aligned} &\left\langle w(z,t), u(z,t), v(z,t), \theta_x(z,t), \theta_y(z,t), \theta_z(z,t), \psi(z,t)\right\rangle \\ &\quad = \left\langle \bar{w}(z), \bar{u}(z), \bar{v}(z), \bar{\theta}_x(z), \bar{\theta}_y(z), \bar{\theta}_z(z), \bar{\psi}(z)\right\rangle e^{i\Omega t} \end{aligned} \tag{8}$$

in which $\bar{w}(z), \bar{u}(z), \bar{v}(z), \bar{\theta}_x(z), \bar{\theta}_y(z), \bar{\theta}_z(z)$ and $\bar{\psi}(z)$ are space functions for longitudinal, transverse, and lateral translations, rotations about the x,y,z axes and warping deformation, respectively. In line with the objective of the paper focusing on steady state response, the displacement fields postulated in Eq. (8) neglect the transient component of the response.

5. Variational formulation

The variational form of the Hamiltonian functional δH is taken to be stationary, i.e.

$$\delta H = \int_{t_1}^{t_2} \delta\left(T^* - U^*\right) dt + \int_{t_1}^{t_2} \delta W^* dt = 0 \tag{9}$$

in which δT^* is the variation of the kinetic energy, δU^* is the variation of internal strain energy and δW^* is the variation of the work done by the applied forces. In Eq. (9), integration is performed between arbitrary time limits t_1 and t_2. The energy variations are given as (e.g., Librescu and Song 2006)

$$\delta T^* = \int_0^\ell \int_A \rho\left(\dot{u}_p \delta\dot{u}_p + \dot{v}_p \delta\dot{v}_p + \dot{w}_p \delta\dot{w}_p\right) dA\, dz \tag{10}$$

$$\delta U^* = \int_0^\ell \int_A E\varepsilon_{zz}\delta\varepsilon_{zz}\, dA\, dz + \int_0^\ell \int_A G\gamma_{zs}\delta\gamma_{zs}\, dA\, dz + \int_0^\ell GJ\theta_z'\delta\theta_z'\, dz \text{ , and} \tag{11}$$

$$\begin{aligned}\delta W^{*} &= N_z(z,t)\,\delta w(z,t)\Big|_0^{\ell} + V_x(z,t)\,\delta u(z,t)\Big|_0^{\ell} + V_y(z,t)\,\delta v(z,t)\Big|_0^{\ell} + M_x(z,t)\,\delta\theta_x(z,t)\Big|_0^{\ell} \\ &+ M_y(z,t)\,\delta\theta_y(z,t)\Big|_0^{\ell} + M_z(z,t)\,\delta\theta_z(z,t)\Big|_0^{\ell} + M_w(z,t)\,\delta\psi(z,t)\Big|_0^{\ell} + \int_0^{\ell}\Big[q_x(z,t)\delta u \\ &+ q_y(z,t)\delta v + q_z(z,t)\delta w + m_x(z,t)\delta\theta_x + m_y(z,t)\delta\theta_y + m_z(z,t)\delta\theta_z + m_w(z,t)\delta\psi\Big]dz\end{aligned} \tag{12}$$

where ρ is the material density, E is the modulus of elasticity, G is the shear modulus, J is the Saint-Venant torsional constant, and A is the cross-sectional area. All primes denote derivatives with respect to space coordinate z while dots denote the derivatives with respect to time. The strain displacement relations based on the small strain assumption are given by

$$\varepsilon_{zz} = \frac{\partial w_p}{\partial z} \quad \text{and} \quad \gamma_{zs} = \frac{\partial \xi}{\partial z} + \frac{\partial w_p}{\partial s} \tag{13}$$

From Eqs. (1)-(8), and by substituting into energy Eqs. (10)-(12), and the resulting expressions into Hamilton's principle (Eq. (9)), performing integration by parts and enforcing the orthogonality conditions; $\left\langle \int_A \left[x(s), y(s), x(s)y(s), x(s)\omega(s), y(s)\omega(s), \omega(s)\right]dA \right\rangle = \langle 0 \rangle$, the governing equations are found to take the form

$$\begin{bmatrix} [\bar{Z}_{11}]_{1\times1} & [0]_{1\times2} & [0]_{1\times4} \\ [0]_{2\times1} & [\bar{Z}_{22}]_{2\times2} & [0]_{2\times4} \\ [0]_{4\times1} & [0]_{4\times2} & [\bar{Z}_{33}]_{4\times4} \end{bmatrix} \begin{Bmatrix} \{\bar{U}_1(z)\}_{1\times1} \\ \{\bar{U}_2(z)\}_{2\times1} \\ \{\bar{U}_3(z)\}_{4\times1} \end{Bmatrix} = \begin{Bmatrix} \{\bar{Q}_1(z)\}_{1\times1} \\ \{\bar{Q}_2(z)\}_{2\times1} \\ \{\bar{Q}_3(z)\}_{4\times1} \end{Bmatrix} \tag{14}$$

where

$$\left\langle \langle \bar{U}_1(z)\rangle^T \,|\, \langle \bar{U}_2(z)\rangle^T \,|\, \langle \bar{U}_3(z)\rangle^T \right\rangle = \left\langle \bar{w}(z) \,|\, \bar{u}(z)\ \bar{\theta}_y(z) \,|\, \bar{v}(z)\ \bar{\theta}_x(z)\ \bar{\theta}_z(z)\ \bar{\psi}(z) \right\rangle$$

$$\left\langle \langle \bar{Q}_1(z)\rangle^T \,|\, \langle \bar{Q}_2(z)\rangle^T \,|\, \langle \bar{Q}_3(z)\rangle^T \right\rangle = \left\langle \bar{q}_z(z) \,|\, \bar{q}_x(z)\ \bar{m}_y(z) \,|\, \bar{q}_y(z)\ -\bar{m}_x(z)\ \bar{m}_z(z)\ \bar{m}_w(z) \right\rangle$$

$$[\bar{Z}_{11}]_{1\times1} = \left[\rho A\,\Omega^2 - EA\,\mathcal{D}^2\right],\quad [\bar{Z}_{22}]_{2\times2} = \begin{bmatrix} -\left(\rho A\,\Omega^2 + GD_{xx}\,\mathcal{D}^2\right) & -GD_{xx}\,\mathcal{D} \\ -GD_{xx}\,\mathcal{D} & \left(EI_{yy}\,\Omega^2 - GD_{xx} + EI_{yy}\,\mathcal{D}^2\right) \end{bmatrix}, \text{ and}$$

$$[\bar{Z}_{33}]_{4\times4} = \begin{bmatrix} -\rho A\,\Omega^2 - GD_{yy}\,\mathcal{D}^2 & -GD_{yy}\,\mathcal{D} & \rho A\,\Omega^2 x_s - GD_{hy}\,\mathcal{D}^2 & -GD_{hy}\,\mathcal{D} \\ & \rho I_{xx}\,\Omega^2 - GD_{yy} + EI_{xx}\,\mathcal{D}^2 & -GD_{hy}\,\mathcal{D} & -GD_{hy} \\ & Symm & -\rho A\,\Omega^2 r_o^2 - G\left(J + D_{\omega\omega}\right)\mathcal{D}^2 & -GD_{\omega\omega}\,\mathcal{D} \\ & & & \rho C_w\,\Omega^2 - GD_{\omega\omega} + EC_w\,\mathcal{D}^2 \end{bmatrix}$$

(15a-e)

where $r_o^2=(1/A)\int_A(h^2+r^2)\,dA=x_s^2+\left(I_{xx}+I_{yy}\right)/A$ is the polar radius of gyration about the shear centre, $\mathcal{D}$ is differential operator $\mathcal{D}\equiv d/dz$ and $\mathcal{D}^2\equiv d^2/dz^2$. The cross-sectional properties arising in Eq. (14) are defined as

$$A, I_{xx}, I_{yy}, C_w, D_{xx}, D_{yy}, D_{hy}, D_{\omega\omega}=\int_A\left[1, y^2, x^2, \omega^2, \left(\frac{dx}{ds}\right)^2, \left(\frac{dy}{ds}\right)^2, \left(\frac{d\omega}{ds}\right)\left(\frac{dy}{ds}\right), \left(\frac{d\omega}{ds}\right)^2\right]dA \quad (16)$$

The boundary terms arising from integration parts of the Hamiltonian functional provide the possible boundary conditions of the problem. They take the form

$$\left[\left(EA\bar{w}'-\bar{N}_z\right)\delta\bar{w}\right]_0^\ell=0,\quad \left[\left(GD_{xx}\left[\bar{u}'-\bar{\theta}_y\right]-\bar{V}_x\right)\delta\bar{u}\right]_0^\ell=0,\quad \left[\left(EI_{yy}\bar{\theta}_y'-\bar{M}_y\right)\delta\bar{\theta}_y\right]_0^\ell=0,$$

$$\left[\left(GD_{yy}\left(\bar{v}'+\bar{\theta}_x\right)+GD_{hy}\left(\bar{\theta}_z'+\bar{\psi}\right)-\bar{V}_y\right)\delta\bar{v}\right]_0^\ell=0,\quad \left[\left(EI_{xx}\bar{\theta}_x'+\bar{M}_x\right)\delta\bar{\theta}_x\right]_0^\ell=0,$$

$$\left[\left(GD_{hy}\left(\bar{v}'+\bar{\theta}_x\right)+G\left(D_{\omega\omega}+J\right)\bar{\theta}_z'+GD_{\omega\omega}\bar{\psi}-\bar{M}_z\right)\delta\bar{\theta}_z\right]_0^\ell=0,\ \left[\left(EC_w\bar{\psi}'+\bar{M}_w\right)\delta\bar{\psi}\right]_0^\ell=0 \quad (17a\text{-}g)$$

The first partition in Eq. (14) provides the governing equation for longitudinal deformation of the member, which is uncoupled from the remaining field equations and can be solved independently. The second partition governs the lateral deflection and associated angle of rotation while the last partition consists of four coupled equations which govern the torsional-flexural response and associated angle of rotation and warping deformations. The first two partitions are observed to be identical to those of the case of doubly symmetric section and the reader is referred to Hjaji and Mohareb (2011a, b) for the solution for such systems. The present study focuses on developing the solution for the response governed by the four coupled torsional-flexural equations provided in third partition $\left[\bar{Z}_{33}\right]\left\{\bar{U}_3(z)\right\}=\left\{\bar{Q}_3(z)\right\}$.

It is noted that the above governing equations are similar to those derived by Laudiero and Savoia (1991) when the shear lag effects and secondary warping terms are omitted, and after replacing the natural frequency terms with the exciting frequency. The present treatment differs from that in Laudiero and Savoia in three respects: (1) Laudiero and Savoia developed an approximate solution based on trigonometric series expansions for the field equations for the case of simply-supported members. In contrast, the present solution explicitly solves the coupled differential equations (in Section 7) and provides solutions applicable to other boundary conditions, (2) while Laudiero and Savoia investigated the free vibration analysis of thin-walled members, the current solution provides the steady state response under general harmonic forces with a given exciting frequency, and (3) in the current study, the closed form solutions derived are used to formulate exact shape functions (Section 7.1) and then develop a super-convergence finite element (Section 7.2). This contrasts with the study in Laudiero and Savoia (1991) which provided only an analytical series solution.

6. Closed form solution

6.1 Homogeneous solution

The homogeneous solution of the system $\left[\bar{Z}_{33}\right]\left\{\bar{U}_3(z)\right\}=\left\{\bar{Q}_3(z)\right\}$ is obtained by setting the right hand side to zero, i.e., $\left\{\bar{Q}_3(z)\right\}=\{0\}$. The homogeneous solution of the space displacement functions $\left\{\bar{U}_{3H}(z)\right\}$ is then assumed to take the exponential form

$$\left\{\bar{U}_{3H}(z)\right\}=\begin{Bmatrix}\bar{v}_h(z)\\ \bar{\theta}_{xh}(z)\\ \bar{\theta}_{zh}(z)\\ \bar{\psi}_h(z)\end{Bmatrix}=\begin{Bmatrix}b_1\\ b_2\\ b_3\\ b_4\end{Bmatrix}_i e^{m_i z} \tag{18}$$

From Eq. (18), by substituting into $\left[\bar{Z}_{33}\right]_{4\times4}\left\{\bar{U}_{3H}(z)\right\}_{4\times1}=\{0\}_{4\times1}$, one obtains

$$\left[\begin{array}{c|c|c|c} -\rho A\Omega^2-GD_{yy}m_i^2 & -GD_{yy}m_i & \rho A\Omega^2 x_s-GD_{hy}m_i^2 & -GD_{hy}m_i \\ \hline & \rho I_{xx}\Omega^2-GD_{yy}+EI_{xx}m_i^2 & -GD_{hy}m_i & -GD_{hy} \\ \hline & Symm & -\rho A\Omega^2 r_o^2-G\left(J+D_{\omega\omega}\right)m_i^2 & -GD_{\omega\omega}m_i \\ \hline & & & \rho C_w\Omega^2-GD_{\omega\omega}+EC_w m_i^2 \end{array}\right]\left\{\begin{array}{c} b_1 \\ \hline b_2 \\ \hline b_3 \\ \hline b_4 \end{array}\right\}_i=\{0\}_{4\times1} \tag{19}$$

where $\langle b\rangle_i^T=\langle b_1 \quad b_2 \quad b_3 \quad b_4\rangle_i$ is a vector of unknown constants corresponding to root m_i. For a non-trivial solution $\{b\}_i$, the determinant of the bracketed matrix in Eq. (19) is set to vanish leading to the bi-quartic equation of the form $B_4m_i^8+B_3m_i^6+B_2m_i^4+B_1m_i^2+B_0=0$,which constants B_0 through B_4 are constants arising from the expansion of the determinant of the 4×4 matrix in Eq. (19) and depend upon cross-sectional properties, material constants, and the exciting frequency and are listed in Appendix A. The above characteristic equation has eight distinct roots m_i (i=1,2,….,8). For each root m_i, there corresponds a set of constants. By back-substitution into the original system of equations $\left[\bar{Z}_{33}\right]_{4\times4}\left\{\bar{U}_{3H}(z)\right\}_{4\times1}=\{0\}_{4\times1}$, one can relate constants $\left(b_1,b_2,b_3\right)_i$ to constant b_{4i} through

$$\begin{Bmatrix}b_1\\ b_2\\ b_3\end{Bmatrix}_i=\begin{Bmatrix}\bar{G}_1\\ \bar{G}_2\\ \bar{G}_3\end{Bmatrix}_i b_{4,i} \tag{20}$$

in which

$$\bar{G}_{1,i}=\frac{Gm_i}{\beta_w}\Big[G^2D_{hy}m_i^2\left(D_{yy}D_{\omega\omega}-D_{hy}^2\right)-D_{hy}\beta_1\left(\rho I_{xx}\Omega^2+EI_{xx}m_i^2\right)$$
$$+\left(\rho A\Omega^2x_s-GD_{hy}m_i^2\right)\left(D_{yy}D_{\omega\omega}-EI_{xx}D_{\omega\omega}m_i^2-G\rho I_{xx}D_{\omega\omega}\Omega^2-GD_{hy}^2\right)\Big]$$

$$\bar{G}_{2,i}=\frac{G}{\beta_w}\Big[\left(\rho A\Omega^2x_s-GD_{hy}m_i^2\right)\left(D_{hy}+Gm_i^2\left[D_{hy}^2+D_{yy}D_{\omega\omega}\right]\right)$$
$$+GD_{hy}D_{\omega\omega}m_i^2\left(\rho A\Omega^2+GD_{yy}m_i^2\right)-\rho A\Omega^2D_{hy}\beta_1\Big]$$

$$\bar{G}_{3,i}=\frac{Gm_i}{\beta_w}\Big[G^2D_{yy}m_i^2\left(D_{hy}^2-D_{yy}D_{\omega\omega}\right)-D_{hy}\left(\rho I_{xx}\Omega^2+EI_{xx}m_i^2\right)\left(\rho A\Omega^2x_s-GD_{hy}m_i^2\right)$$
$$-\left(\rho A\Omega^2+GD_{yy}m_i^2\right)\left(D_{\omega\omega}\beta_o+GD_{hy}^2\right)\Big] \qquad (21a\text{-}c)$$

where

$$\beta_o=\rho I_{xx}\Omega^2+EI_{xx}m_i^2-GD_{yy},\quad \beta_1=\rho A\Omega^2r_o^2+G\left(J+D_{\omega\omega}\right)m_i^2 \quad \text{, and}$$

$$\beta_w=\left(\rho A\Omega^2x_s-GD_{hy}m_i^2\right)\left(2G^2D_{hy}D_{yy}m_i^2-\beta_o\rho A\Omega^2x_s+G\beta_oD_{hy}m_i^2\right)$$
$$+\left(\rho A\Omega^2+GD_{yy}m_i^2\right)\left[G^2D_{hy}^2m_i^2+\beta_o\beta_1\right]+\beta_1\left(GD_{yy}m_i\right)^2$$

Eq. (20) reduces the number of unknown constants from 32 to 8 independent constants. From Eq. (20) by substituting into Eq. (18), the homogeneous solution is obtained as

$$\left\{\bar{U}_{3H}(z)\right\}_{4\times1}=\left[\chi(z)\right]_{4\times8}\left\{\bar{B}\right\}_{8\times1}=\left[\bar{G}\right]_{4\times8}\left[\bar{E}(z)\right]_{8\times8}\left\{\bar{B}\right\}_{8\times1} \qquad (22)$$

in which

$$\left[\bar{G}\right]_{4\times8}=\left[\begin{Bmatrix}\bar{G}_{1,1}\\ \bar{G}_{2,1}\\ \bar{G}_{3,1}\\ 1\end{Bmatrix}\middle|\middle|\begin{Bmatrix}\bar{G}_{1,2}\\ \bar{G}_{2,2}\\ \bar{G}_{3,2}\\ 1\end{Bmatrix}\middle|\middle|\begin{Bmatrix}\bar{G}_{1,3}\\ \bar{G}_{2,3}\\ \bar{G}_{3,3}\\ 1\end{Bmatrix}\middle|\middle|.....\middle|\middle|\begin{Bmatrix}\bar{G}_{1,8}\\ \bar{G}_{2,8}\\ \bar{G}_{3,8}\\ 1\end{Bmatrix}\right],$$

matrix $\left[\bar{E}(z)\right]_{8\times8}$ is a diagonal matrix consisting of the exponential functions e^{m_iz} $(i=1,2,....,8)$, the vector of constants $\left\langle\bar{B}\right\rangle_{1\times8}^T=\left\langle b_{4,1},b_{4,2},b_{4,3},.....,b_{4,8}\right\rangle$ is to be determined from the boundary conditions of the problem, and the matrix $\left[\chi(z)\right]_{4\times8}=\left[\bar{G}\right]_{4\times8}\left[\bar{E}(z)\right]_{8\times8}$ relating the homogeneous solution to the integration constants has been introduced.

6.2 Special case: particular solution for uniform member loads

For a member under uniform distributed loads, $\left[\bar{q}_y(z),\bar{m}_x(z),\bar{m}_z(z),\bar{m}_w(z)\right]e^{i\Omega t}=\left[\bar{q}_y,\bar{m}_x,\bar{m}_z,\bar{m}_w\right]e^{i\Omega t}$, the corresponding particular solution $\left\{\bar{U}_{3P}(z)\right\}_{4\times1}$ is given as

$$\left\{\overline{U}_{3P}\right\}_{4\times1}=\begin{Bmatrix}\overline{v}_p\\ \overline{\theta}_{xp}\\ \overline{\theta}_{zp}\\ \overline{\psi}_p\end{Bmatrix}_{4\times1}=\begin{Bmatrix}\dfrac{r_o^2\overline{q}_y+x_s\overline{m}_z}{\rho A\,\Omega^2\left(x_s^2-r_o^2\right)}\\ \dfrac{\left(\rho C_w\,\Omega^2-GD_{\omega\omega}\right)\overline{m}_x-GD_{hy}\,\overline{m}_w}{G^2D_{hy}^2-\left(\rho I_{xx}\,\Omega^2-GD_{yy}\right)\left(\rho C_w\,\Omega^2-GD_{\omega\omega}\right)}\\ \dfrac{x_s\overline{q}_y+\overline{m}_z}{\rho A\,\Omega^2\left(x_s^2-r_o^2\right)}\\ \dfrac{GD_{hy}\,\overline{m}_x-\left(\rho I_{xx}\,\Omega^2-GD_{yy}\right)\overline{m}_w}{G^2D_{hy}^2-\left(\rho I_{xx}\,\Omega^2-GD_{yy}\right)\left(\rho C_w\,\Omega^2-GD_{\omega\omega}\right)}\end{Bmatrix}_{4\times1} \tag{23}$$

6.3 Total solution for uniform member loads

The total steady state response is obtained by adding the homogeneous solution in Eq. (22) to the particular solution in Eq. (23), yielding

$$\left\{\overline{U}_3(z)\right\}_{4\times1}=\left[\chi(z)\right]_{4\times8}\left\{\overline{B}\right\}_{8\times1}+\left\{\overline{U}_{3P}\right\}_{4\times1} \tag{24}$$

Integration constants $\left\{\overline{B}\right\}$ appearing in Eq. (24) are determined from the boundary conditions. As an example, Appendix B provides the vector $\left\{\overline{B}\right\}$ for the case of a cantilever subjected to uniform member loads and concentrated tip loads as an example.

7. Finite element formulation

The finite element sought has two nodes with four degrees of freedom per node. Displacement fields $\left\langle\overline{U}_{3H}(z)\right\rangle_{1\times4}^T=\left\langle\overline{v}_h(z)\overline{\theta}_{xh}(z)\overline{\theta}_{zh}(z)\overline{\psi}_h(z)\right\rangle_{1\times4}$ are thus to be expressed in terms of nodal displacements $\left\langle U_N\right\rangle_{1\times8}^T=\left\langle v_1\theta_{x1}\theta_{z1}\psi_1v_2\theta_{x2}\theta_{z2}\psi_2\right\rangle_{1\times8}$.

7.1 Formulating shape functions

Shape functions which exactly satisfy the homogeneous part of the coupled field equations are formulated through

$$\{U_N\}_{8\times1}=\begin{Bmatrix}\{\overline{U}_{3H}(0)\}_{4\times1}\\ \{\overline{U}_{3H}(l)\}_{4\times1}\end{Bmatrix}=\begin{bmatrix}[\chi(0)]_{4\times8}\\ [\chi(l)]_{4\times8}\end{bmatrix}\{\overline{B}\}_{8\times1}=[L]_{8\times8}\{\overline{B}\}_{8\times1} \tag{25}$$

Eq. (25) is solved for vector $\left\{\overline{B}\right\}$ and then substituted into Eq. (24), yielding

$$\left\{\,\overline{U}_{3H}(z)\right\}_{4\times1}=\left[\chi(z)\right]_{4\times8}\left[L\right]_{8\times8}^{-1}\left\{\,U_N\right\}_{8\times1}=\left[\,H(z)\right]_{4\times8}\left\{\,U_N\right\}_{8\times1} \tag{26}$$

in which $\left[H(z)\right]_{4\times8}=\left[\chi(z)\right]_{4\times8}\left[L\right]^{-1}_{8\times8}$ is a matrix of shape functions which exactly satisfy the homogeneous form of the equilibrium equations. Such shape functions will be shown to avoid mesh discretization errors appearing in most finite elements. Also, it yields an element that is free of shear locking.

7.2 Matrix formulation

Eqs. (1)-(4) are substituted into Eq. (13) to express the longitudinal and shear strain relations in terms of displacement fields. The resulting expressions are substituted into Eqs. (6)-(8) to express the variation of energy expressions given in Eqs. (10)-(12). Eq. (26) is substituted into Eq. (9) and the orthogonality conditions $\int_A\left[x\,,y\,,xy\,,x\,\omega,y\,\omega,\omega\right]dA=0$ are evoked yielding

$$([K_e]_{8\times8}-\Omega^2[M_e]_{8\times8})\{U_N\}_{8\times1}=\{F_e\}_{8\times1} \tag{27}$$

in which the stiffness matrix $[K_e]_{8\times8}$ is given by

$$[K_e]_{8\times8}=\int_0^l([H'(z)]^T_{8\times4}[Y_a]_{4\times4}[H'(z)]_{4\times8}+[H_s(z)]^T_{8\times4}[Y_s]_{4\times4}[H_s(z)]_{4\times8})dz \tag{28}$$

where

$$\left[H_s(z)\right]^T_{8\times4}=\left[\left\{H'_{1,j}(z)\right\}_{8\times1}\left\{H_{2,j}(z)\right\}_{8\times1}\left\{H'_{3,j}(z)\right\}_{8\times1}\left\{H_{4,j}(z)\right\}_{8\times1}\right]^T,$$

$$\left[Y_a\right]_{4\times4}=Diag\left[0\mid EI_{xx}\mid GJ\mid EC_w\right]\quad\text{, and}$$

$$[Y_s]_{4\times4}\begin{bmatrix}GD_{yy} & GD_{yy} & GD_{hy} & GD_{hy}\\ & GD_{yy} & GD_{hy} & GD_{hy}\\ & Symm & GD_{\omega\omega} & GD_{\omega\omega}\\ & & & GD_{\omega\omega}\end{bmatrix}_{4\times4}$$

Also, in Eq. (27), the mass matrix $[M_e]_{8\times8}$ is given by

$$[M_e]_{8\times8}=\int_0^l([H'(z)]^T_{8\times4}[X_m]_{8\times4}[H(z)]_{4\times8}+[H_s(z)]^T_{8\times4}\,dz \tag{29}$$

in which

$$[X_m]_{4\times4}\begin{bmatrix}\rho A & 0 & -x_s & 0\\ 0 & \rho I_{xx} & 0 & 0\\ -x_s & 0 & \rho A r_0^2 & 0\\ 0 & 0 & 0 & \rho C_w\end{bmatrix}_{4\times4}$$

and the energy equivalent load vector $\left\{F_e(z)\right\}_{8\times1}$ is given by

$$\left\{F_e(z)\right\}_{8\times1}=\int_0^\ell\left[H(z)\right]^T_{8\times4}\left\{\bar{Q}_3(z)\right\}_{4\times1}dz \tag{30}$$

8. Examples and discussion

While the above formulation provides the response under harmonic loads, it can also approach the response under static loads when adopting a very low exciting frequency Ω compared to the first natural frequency $\bar{\omega}_1$ of the system (e.g., $\Omega \approx 0.01\,\bar{\omega}_1$). Three examples are investigated for beams with a variety of cross-sections, loading and boundary conditions. Material is assumed to be steel with (E=200 GPa, G=77 GPa and ρ=7850 kg/m^3). The finite element solution developed in the present study is based on the shapes functions which exactly satisfy the homogeneous form of the governing field equations. This treatment eliminates mesh discretization errors in conventional finite element solutions based on polynomial shape functions. As a result, it was observed that solutions based on a single finite element per span yielded results exactly matching those based on closed-from solutions provided in Appendix B up to five significant digits. Additional solutions were provided for comparison. These are:

(i) A Vlasov beam theory solution which neglects shear deformation and distortional effects,

(ii) An Abaqus two-noded B31OS beam element with seven degrees of freedom per node (i.e.,three translation, three rotations and warping deformation) which accounts for shear deformation due to only bending but omits (a) shear deformation effects due to warping deformation and (b) distortional effects, and

(iii) An Abaqus S4R shell element solution (shell element with four nodes with six degrees of freedom per node, i.e., three translation and three rotations, and reduced integration) which captures shear deformation and distortional effects.

8.1 Example 1 – long cantilever under uniformly distributed torsion

A 4m span cantilever beam with monosymmetric I-section is subjected to uniformly distributed harmonic torsion $m_z(z,t)=1.80e^{i\Omega t}$ kNm/m is considered (Fig. 2). The dimensions of the cross-section are; flange thickness t_f=20 mm, web thickness t_w=15 mm, upper flange width b_u=100 mm, lower flange width b_l=200 mm and a middle surface height H=200 mm. It is required to (1) conduct a steady state analysis and extract the natural frequencies, (2) conduct a quasi-state analysis by adopting an exciting frequency $\Omega \approx 0.01\,\bar{\omega}_1$=0.4415 rad/sec, and (3) conducting a steady state dynamic response $\Omega = 1.423\,\bar{\omega}_1 \approx$62.83 rad/sec.

The shear centre S_c coordinate along the axis of symmetry is x_s=−55.56 mm, and the coordinate of the centroid in the direction of the principle axis of symmetry is C_x=77.78 mm. The section properties are: $A=0.56\times10^4$ mm^2, $I_{xx}=15.0\times10^6$ mm^4, $J=1.025\times10^6$ mm^4, $C_w=59.26\times10^9$ mm^6, $D_{yy}=0.60\times10^4$ mm^2, $D_{hy}=26.67\times10^3$ mm^3, $D_{\omega\omega}=65.19\times10^6$ mm^4.

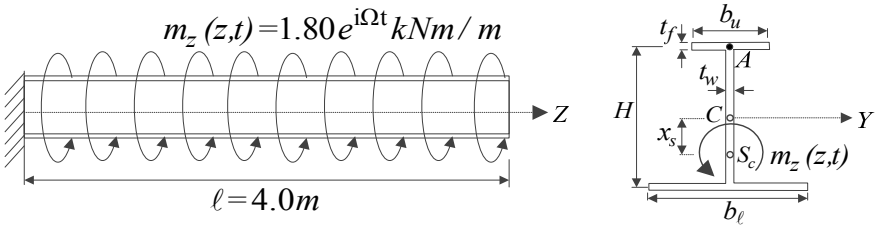

Fig. 2 Cantilever with mono-symmetric I-section under distributed harmonic Torsion

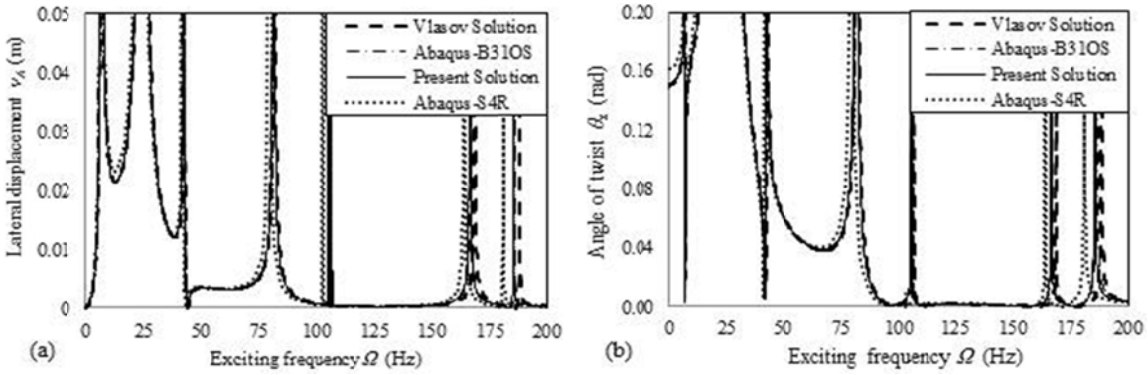

Fig. 3 Steady state response of cantilever monosymmetric under distributed harmonic torsion (a) Lateral displacement $\bar{v}_A$, (b) Angle of twist $\bar{\theta}_z$

Table 1 Natural frequencies of cantilever beam of monosymmetric I-section

Mode	Abaqus S4R [1]	Present Solution [2]	Abaqus B31OS [3]	Vlasov Solution [4]	Present Difference =[1-2]/1	B31OS Difference =[1-3]/1	Vlasov Difference =[1-4]/1
1	7.041	7.082	7.093	7.098	-0.58%	-0.74%	-0.81%
2	24.02	24.69	24.70	24.73	-2.79%	-2.83%	-2.96%
3	41.95	42.28	42.56	42.69	-0.79%	-1.45%	-1.76%
4	79.93	81.51	81.70	82.05	-1.98%	-2.21%	-2.65%
5	103.1	105.2	105.7	106.5	-2.04%	-2.52%	-3.30%
6	164.0	165.8	167.1	168.8	-1.10%	-1.89%	-2.93%
7	181.4	185.8	186.5	188.6	-2.43%	-2.81%	-3.97%

In the Abaqus model, a total of 3,520 S4R shell elements are used (i.e., 4 elements per upper flange, 8 elements per bottom flange, 10 elements along the web height and 160 elements along the longitudinal axis) while in the case of Abaqus B31OS beam element, a total of 100 elements along the cantilever axis are used.

8.1.1 Steady state analysis

Under uniformly distributed harmonic twisting moment, $m_z(z,t)=1.80e^{i\Omega t}$ kNm/m, the natural frequencies related to coupled lateral-torsional response can be extracted from the steady state response analysis as illustrated in Fig. 3(a)-(b). Fig. 3(a)-(b) show the peak lateral displacement and angle of twist at the cantilever tip as a function of the exciting frequency. The solution is based on the element developed in the present study. Overlaid on the same plots are solutions based on (1) the Vlasov theory, (2) Abaqus B31OS beam element using 100 elements and (3) Abaqus S4R shell element using 3,520 elements for comparison. The exciting frequency was varied from nearly zero to 200 Hz. Peaks on both diagrams indicate resonance and are thus indicators of the natural frequencies of the beam. It is noted that lateral displacement peaks are synchronized with the angle of twist peaks indicating that the mode shape is indeed coupled lateral-torsional. Excellent agreement is obtained between all solutions.

Table 1 provides the first seven natural frequencies extracted from the analysis. Close agreement is observed between all four solutions, particularly at lower natural frequencies. For

Table 2 Quasi-static analysis of cantilever with monosymmetric I-section

Variable	Abaqus S4R [1]	Present Solution [2]	Abaqus B31OS [3]	Vlasov Solution [4]	Present Difference =[1-2]/1	B31OS Difference =[1-3]/1	Vlasov Difference =[1-4]/1
$\bar{v}_A$ (mm)	-28.53	-26.87	-26.85	-26.77	5.82%	5.89%	6.17%
$\bar{\theta}_z$ (10^{-3} rad)	159.3	151.4	151.2	150.1	4.96%	5.08%	5.78%
$\bar{\psi}$ (10^{-6} rad/mm)	11.03	9.061	8.954	8.796	17.85%	18.82%	20.25%

higher natural frequencies, predictions by the Vlasov theory were the highest followed by the B31OS solution, followed by the present solution, while the frequencies predicted by ABAQUS were the lowest. This is a natural outcome of the fact that the Vlasov beams provides the stiffest representation of the beam (since it ignores shear deformation and distortional effects) while that based on ABAQUS shell analysis provides the most flexible one given the large number of degrees of freedom involved. The frequencies predicted by the present solution differed from 0.58% to 2.43% from those based on ABAQUS and provides the closest agreement with the shell solution.

8.1.2 Quasi-static solution

Table 2 shows the quasi-static response results for maximum lateral displacement $\bar{v}_A$ of point A (Fig. 2), associated bending rotation $\bar{\theta}_x$, twist angle $\bar{\theta}_z$ and the warping deformation function $\bar{\psi}$. Results are based on (a) the solutions (closed form and finite element) developed in the present study, (b) Vlasov beam theory and (c) Abaqus B31OS-beam and S4R-shell elements. Results based on the present study are observed to nearly coincide with those based on the Vlasov beam theory and Abaqus-B31OS beam element, but slightly depart from the Abaqus shell element. The lateral displacement $\bar{v}_A$, and twist angle $\bar{\theta}_z$ were respectively found 5.82% , 4.96% lower than those based on Abaqus S4R-shell model. The differences are attributed to cross-section distortional effects which are captured in Abaqus shell element solution but not in the other three solutions.

In order to extract the bending rotation $\bar{\theta}_x$ and warping deformation $\bar{\psi}$ from the finite element model at a given section *z*, the top flange rotation $\bar{\theta}_t$ and bottom flange rotation $\bar{\theta}_b(z)$ about the *x* axis were extracted from the model. Eq. (1) is then applied at the bottom flange (by setting $x=h_b$, h_b being the distance from the shear centre to the bottom flange), leading to $w_b(z,y,t)=w(z,t)+y\theta_x(z,t)-h_b\theta_y(z,t)+h_b y\psi(z,t)$. Eq. (8) is then used to express the steady state component of the displacement response leading to $\bar{w}_b(z,x)\Rightarrow\bar{w}(z)+y\,\bar{\theta}_x(z)-h_b\,\bar{\theta}_y(z)+h_b y\,\bar{\psi}(z)$. The bottom flange rotation is then obtained by differentiation with respect to coordinate *y* yielding $\bar{\theta}_b(z)=\partial\bar{w}_b/\partial x=\bar{\theta}_x(z)+h_b\bar{\psi}(z)$. A similar treatment for the top flange yields $\bar{\theta}_t(z)=\partial\bar{w}_t/\partial x=\bar{\theta}_x(z)-h_t\bar{\psi}(z)$, h_t being the distance from the shear centre to the top flange. Knowing $\bar{\theta}_t(z)$ and $\bar{\theta}_b(z)$ from the finite element model and the distances h_t and h_b, one can calculate the angle of rotation $\bar{\theta}_x(z)$ and the warping deformation $\bar{\psi}(z)$ for the section of interest z as predicted by finite element. The above procedure has led to the warping deformation entry $\bar{\psi}$ in the last row of Column [1] which is subsequently used as a basis to compare the warping deformations obtained in other beam solutions. Again, the closest prediction to FEA results is that based on the present study which underestimated the warping deformation $\bar{\psi}$ by 17.85%. This

compares to a 20.25% difference for the Vlasov theory. Under the applied quasi-static loading, $\bar{\theta}_x(z)$ was observed to vanish in all four solutions. Under the Vlasov and the B31OS solutions subject to static twisting moments, $\bar{\theta}_x(z)$ are expected to vanish since there is no coupling between the flexural and twisting mode. Under the present theory, the presence of non-zero terms on the off-diagonal terms of the field equations (Eq. (15e)) suggest that, in principle, coupling should exist between twist and lateral deformation. The coupling is due to two factors: (1) shear deformation effects (evidenced by the presence of the term GD_{hy} on the off-diagonal term), and (2) the presence of harmonic forces (given the dependence of the off-diagonal terms on the exciting frequency). As a general observation, the present solution is successful at capturing the static response of the system.

8.1.3 Steady state dynamic response

For the exciting frequency $\Omega = 1.423\bar{\omega}_1 \approx 62.83 \text{rad/sec}$, Fig. 4(a)-(d) show the lateral displacement $\bar{v}_A(z)$, associated bending rotation $\bar{\theta}_x(z)$, angle of twist $\bar{\theta}_z(z)$ and warping deformation $\bar{\psi}(z)$. Results are in excellent agreement with the Vlasov beam theory and Abaqus B31OS but slightly differ from Abaqus S4R shell model which exhibits a slightly more flexible response. Again, the difference is attributed to cross-sectional distortional effects.

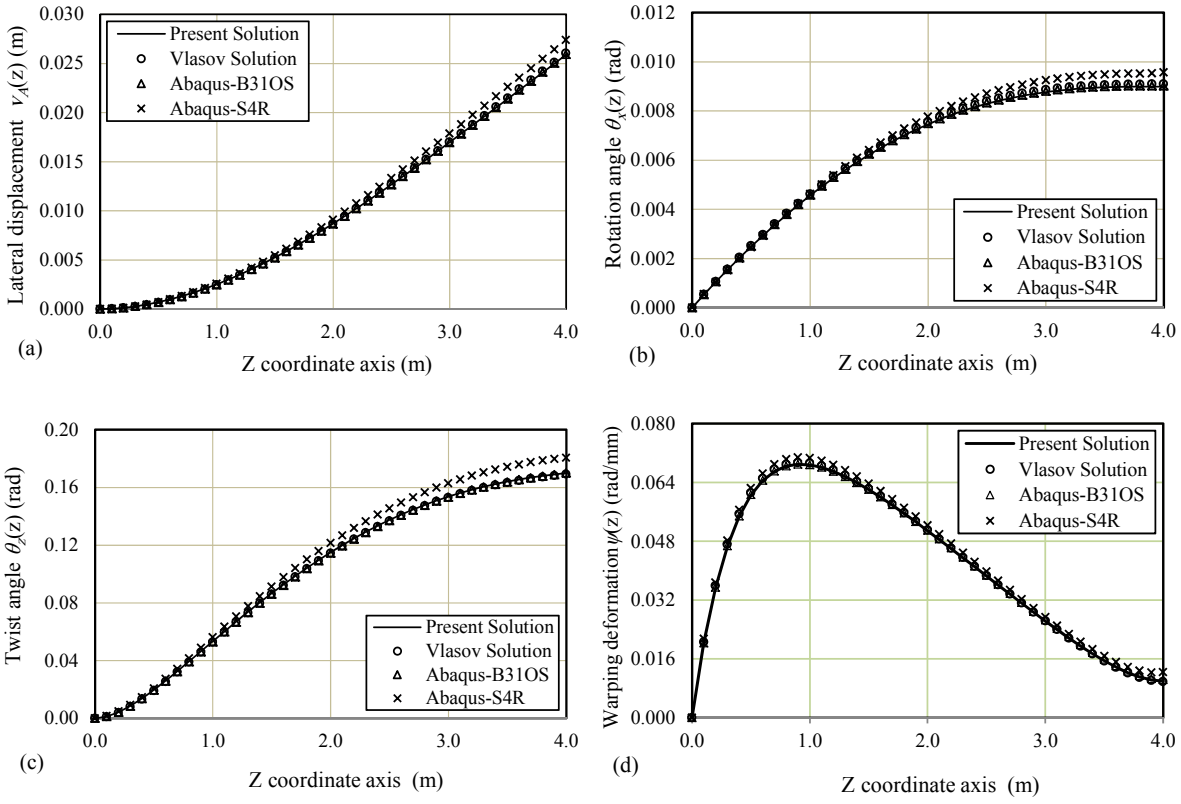

Fig. 4 Steady state response for cantilever monosymmetric I-section under distributed harmonic torsion

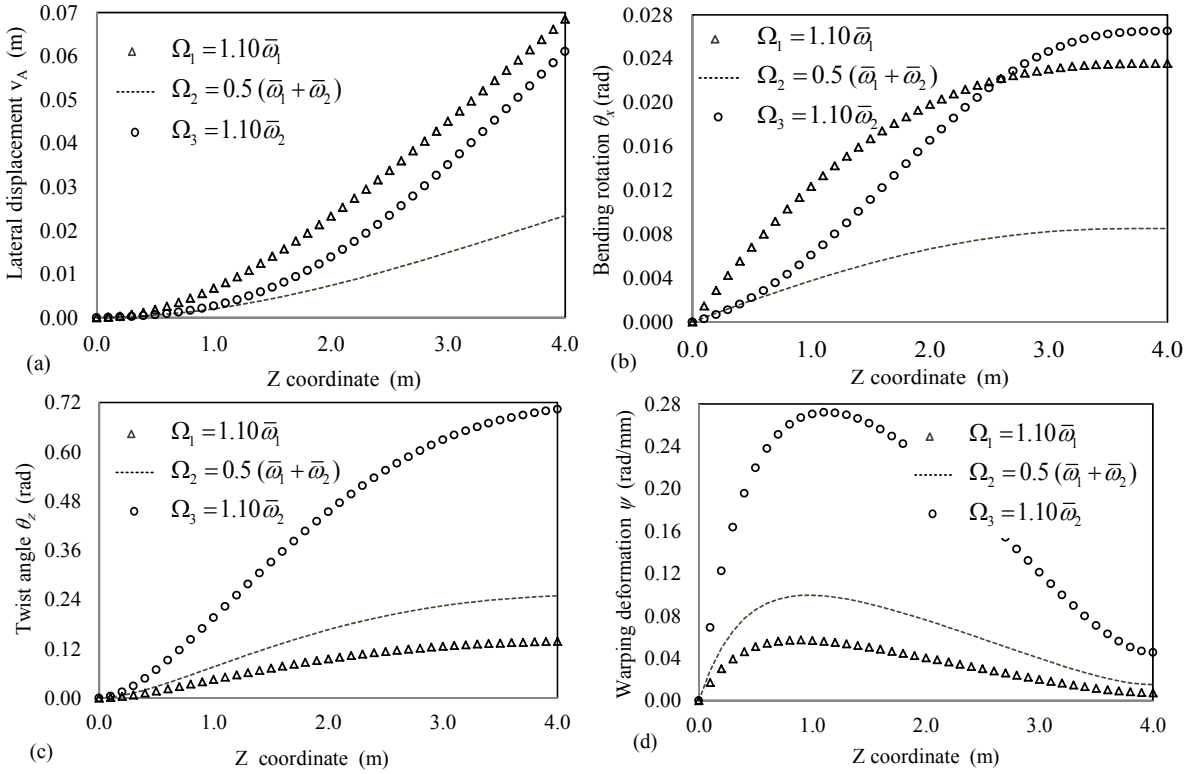

Fig. 5 (a) Lateral displacement, (b) bending rotation, (c) twist angle, (d) warping deformation function responses for cantilever monosymmetric I-section

The peak displacement responses corresponding to three frequencies $\Omega_1 = 1.10\bar{\omega}_1$, $\Omega_2 = 0.5(\bar{\omega}_1 + \bar{\omega}_2)$ and $\Omega_3 = 1.10\bar{\omega}_2$ are plotted in Fig. 5. Given the proximity of the exciting frequencies Ω_1 to the first natural frequency and Ω_3 to the third natural frequency, the corresponding deformation responses assume a shape close to the first two natural modes of vibration. The exciting frequency $\Omega_2 = 0.5(\bar{\omega}_1 + \bar{\omega}_2)$ lies between both natural frequencies. Thus, the corresponding deformation response can be conceived essentially as a linear combination of the first and second modes of vibrations as depicted on the figure. Also, since the exciting frequency Ω_2 is far from both natural frequencies $\bar{\omega}_1$, $\bar{\omega}_2$, resonance does not take place and the magnitude of the displacements are generally smaller than those based on the exciting frequencies $\Omega_1 = 1.10\bar{\omega}_1$ and $\Omega_3 = 1.10\bar{\omega}_2$.

8.2 Example 2 - effect of shear deformation

The purpose of this example is to illustrate the ability of the element developed in the present study to capture shear deformation effects in the coupled lateral-torsional response of short cantilever spanning 0.8 m. The cantilever has the same cross-section as that given in Example 1 and is subjected to a uniformly distributed harmonic torsion $m_z(z,t)=1.50e^{i\Omega t}$ kNm/m acting along the beam axis as shown in Fig. 6. Two exciting frequencies $\Omega = 0.001\bar{\omega}_1$ rad/sec and

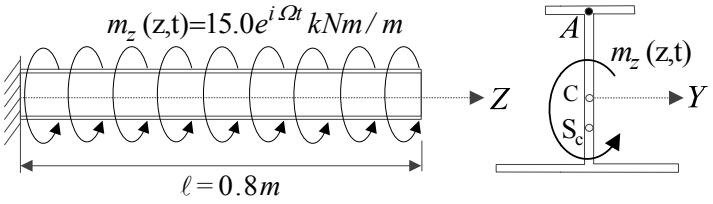

Fig. 6 Cantilever with monosymmetric I-section under member harmonic torsion

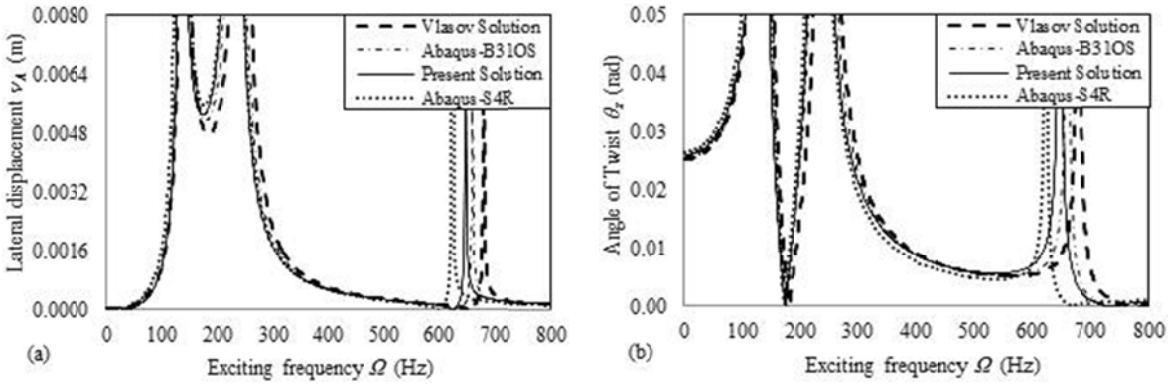

Fig. 7 Natural frequency analysis of short cantilever monosymmetric I-section; (a) Lateral displacement $\bar{v}_A$ and (b) Angle of twist $\bar{\theta}_z$

$\Omega \approx 1.37\bar{\omega}_1$ rad / sec are considered to investigate the quasi-static and steady state dynamic analyses of the short beam. The first natural frequency of the short cantilever is $\bar{\omega}_1$=131.4 Hz. In order to validate of the present solutions (i.e. closed-form solution and finite element formulation based on a single element), Abaqus model solutions based on B31OS-beam and S4R-shell elements are presented while the influence of shear deformation is exhibited by comparison with classical Vlasov beam solution.

8.2.1 Natural frequency extraction

A steady state analysis is conducted based on the present solution (with a single element). Results based on Vlasov theory, the Abaqus B31OS beam element (with 40 elements) and shell element (with 880 elements) are provided for comparison. The lateral displacement at the cantilever tip is plotted versus the exciting frequency in Fig. 7(a). Also, the angle of twist versus the exciting frequency is plotted in Fig. 7(b). Again, since the response is coupled, the peak lateral displacements are observed to be synchronized with those of the natural frequency values of the beam (Table 3). All four solutions closely predict the location the first peak corresponding to the fundamental frequency. For higher frequencies, some discrepancy in the location of the peak response becomes apparent between the four solutions. For the third mode of vibration, the Abaqus shell model predicts the lowest natural frequency, followed by the present solution, followed by Abaqus B31OS while the highest frequency is predicted by Vlasov solution. This is expected since (a) for higher modes, shear deformation is known to have a higher influence (Chen and Lui 1997), and (b) distortional effects become more prominent. Compared to the shell solution, the present solution overpredicts the third natural frequency by 7.59%, followed by B31OS by 9.54% since

Table 3 Natural frequencies of cantilever monosymmetric I-section under member harmonic torsion

Mode	Abaqus S4R [1]	Present Solution [2]	Abaqus B31OS [3]	Vlasov Solution [4]	Present Difference =[1-2]/1	B31OS Difference =[1-3]/1	Vlasov Difference =[1-4]/1
1	131.4	136.6	137.3	138.5	-3.96%	-4.49%	-5.40%
2	229.3	230.1	236.5	244.6	-0.35%	-3.14%	-6.67%
3	602.5	648.2	660.0	680.3	-7.59%	-9.54%	-12.91%

Table 4 Static response of short cantilever monosymmetric I-section under distributed harmonic torsion

Variable	Abaqus S4R [1]	Present Solution [2]	Abaqus B31OS [3]	Vlasov Solution [4]	Present Difference =[1-2]/1	B31OS Difference =[1-3]/1	Vlasov Difference =[1-4]/1
$\bar{v}_A$ (mm)	5.299	4.655	4.557	4.462	12.15%	14.00%	15.80%
$\bar{\theta}_z$ (10^{-3} rad)	27.15	25.97	25.77	25.19	4.86%	5.08%	7.26%
$\bar{\psi}$ (10^{-6} rad/mm)	35.72	33.78	33.85	33.34	5.43%	5.24%	6.66%

Table 5 Steady state response of cantilever monosymmetric I-section under distributed harmonic torsion

Variable	Abaqus S4R [1]	Present Solution [2]	Abaqus B31OS [3]	Vlasov Solution [4]	Present Difference =[1-2]/1	B31OS Difference =[1-3]/1	Vlasov Difference =[1-4]/1
$\bar{v}_A$ (mm)	5.784	5.605	5.421	4.801	3.09%	6.28%	17.00%
$\bar{\theta}_x$ (10^{-3} rad)	8.995	8.963	8.822	8.268	0.36%	1.92%	8.08%
$\bar{\theta}_z$ (10^{-3} rad)	4.693	4.454	4.375	3.818	5.09%	6.78%	18.64%
$\bar{\psi}$ (10^{-6} rad/mm)	-6.406	-6.152	-5.470	-4.863	3.97%	14.61%	24.09%

both do not capture distortional effects, while the Vlasov solution overpredicts the solution by 12.91% since it captures neither distortion nor shear deformation.

8.2.2 Comparison of displacement responses

A comparison between the displacement responses of all four solutions are provided in Table 4 for the quasi-static case and Table 5 for the dynamic case. In both cases, the best agreement with the Abaqus shell solution is obtained in the case of the present solution. For the static case, the difference is 12.15% for the lateral displacement, 4.86% for the angle of twist, and 5.43% for the warping deformation. Again, the bending rotation $\bar{\theta}_x$ nearly vanished in all four solutions. For the steady state dynamic case, the present study predicts displacement $\bar{v}_A$, bending rotation $\bar{\theta}_x$, angle of twist $\bar{\theta}_z$ and warping deformation $\bar{\psi}$ that are respectively 3.09%, 0.36%, 5.09% and 3.97% lower than those based on the Abaqus shell element model. These percentages respectively correspond to 17.00%, 8.08%, 18.64% and 24.09% for the Vlasov theory (as listed in the last column of the table). Thus, the present theory provides a significantly more accurate response compared to that of Abaqus. The differences are due to the effects of shear deformation which are incorporated in the present theory but not in Vlasov theory. The results provided in Tables 4 and 5 show that shear deformation effects are more important in the steady state dynamic response analysis than they are for static analysis.

Fig. 8 shows the displacement response for the case of harmonic loading. The present

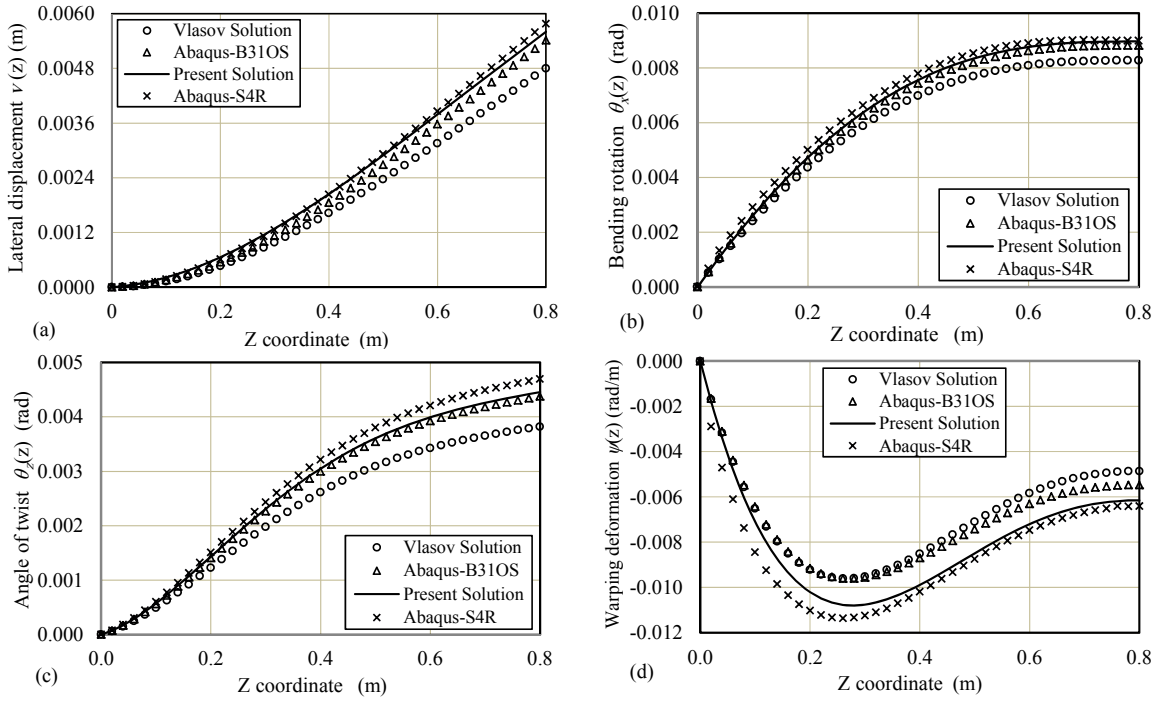

Fig. 8 Dynamic analysis of short cantilever under member harmonic torsion; (a) lateral displacement, (b) bending rotation, (c) twist angle, and (d) warping deformation

theory/finite element is observed to be in excellent agreement with the Abaqus S4R shell solution. The omission of shear deformation effects in the other two solutions (either fully in the Vlasov theory or partially in the Abaqus B31OS) results in some discrepancy in the predicted displacement response. This was observed to particularly be the case of short beams under harmonic forces.

8.3 Example 3 – continuous span beam

A three-span beam (Fig. 9) with a channel-section subjected to three harmonic forces; concentrated transverse force $P_y(z,t)=16.0e^{i\Omega t}$ kN, concentrated torsion $M_z=15.4e^{i\Omega t}$ kN/m and uniformly distributed transverse force $q_y=8.0e^{i\Omega t}$ kN/m is considered. The exciting frequency is assumed to take two values $\Omega\approx 0.001\,\overline{\omega}_1$ (quasi-static) and $\Omega\approx 2.38\,\overline{\omega}_1$, where the first natural frequency in the present problem is $\overline{\omega}_1=58.06$ rad/sec. The dimensions of the C-section are: t_f=20 mm, t_w=12 mm, b=80 mm, H=20 mm, x_s=−54.86 mm, C_x=22.86 mm, C_y=100 mm, and the C-section properties are: $A=0.56\times10^4$ mm^2, $I_{xx}=40.0\times10^6$ mm^4, $J=0.54\times10^6$ mm^4, $C_w=27.31\times10^9$ mm^6, $D_{yy}=0.24\times10^4$ mm^2, $D_{hy}=76.60\times10^3$ mm^3 and $D_{\omega\omega}=34.46\times10^6$ mm^4. It is required to compare the static and steady state responses based on the finite element with the beam solution.

Only five elements were needed to model the problem. This is a natural outcome of the use of exact shape functions in the formulation (which eliminate any mesh discretization errors). In contrast, the Abaqus B31OS solution model, one hundred beam elements were needed to eliminate discretization errors.

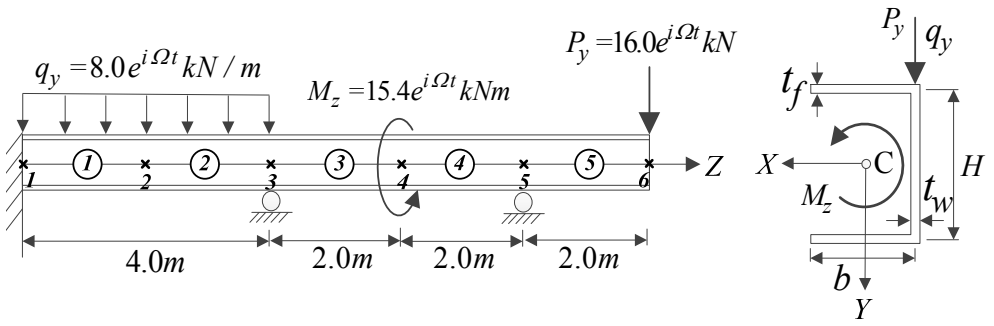

Fig. 9 Continuous beam with channel-section under harmonic forces

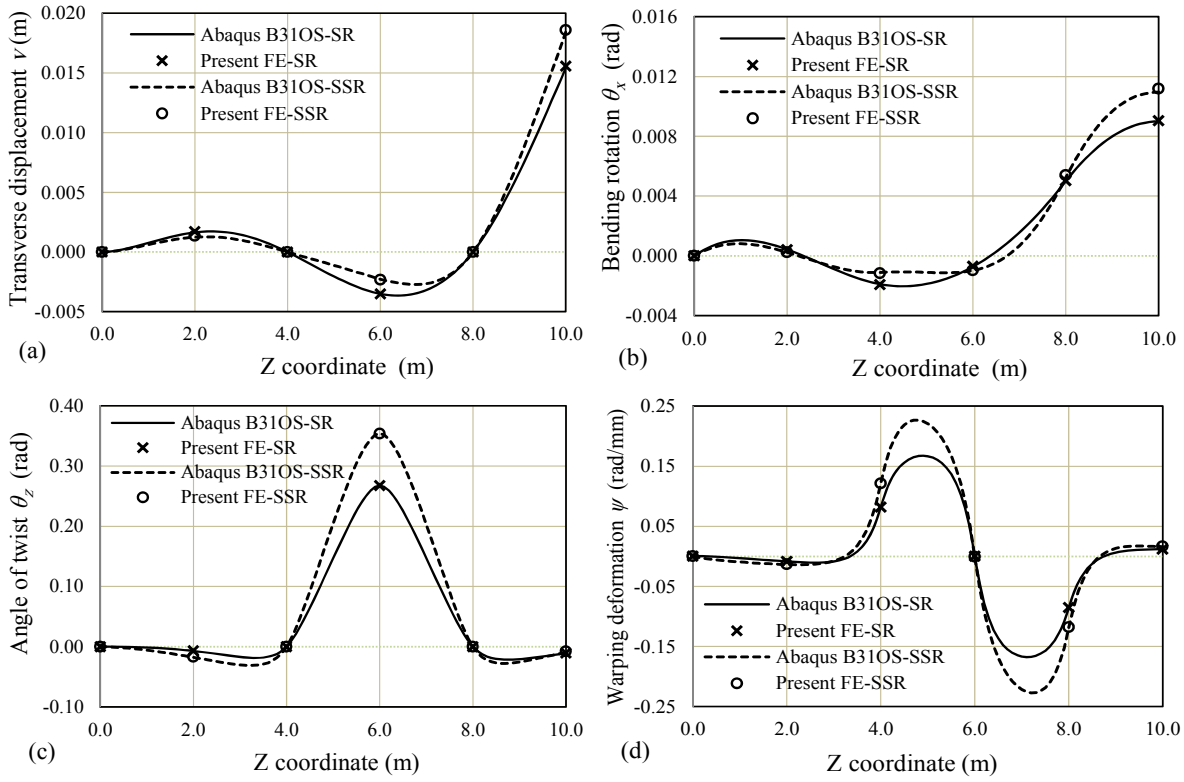

Fig. 10 Static and dynamic analyses of three-span continuous beam under general harmonic forces

The corresponding generalized displacement diagrams are shown in Fig. 10(a)-(d), in which the quasi-static response is denoted (SR) and the steady state response based on Ω=2.38$\overline{\omega}_1$ is denoted (SSR). It is observed that the present finite element formulation results based on five beam elements provide an excellent agreement with that based on the Abaqus solution at a fraction of the computational and modelling cost.

9. Conclusions

• A super-convergent finite element formulation was developed for beams with mono-symmetric sections. The element is based on shape functions which exactly satisfy the homogeneous form of the equilibrium equations and thus eliminates the discretization errors encountered under other interpolation schemes. The solution captures shear deformation effects, warping, translational and rotary inertial effects.

• The solution is able to efficiently capture the static and steady state response of beams under harmonic loads. The steady state response is obtained without the need to extract the eigen-modes. The solution is capable of extracting the eigen-frequencies and eigen-modes, when needed.

• The formulation successfully captures the coupled lateral-torsional response of mono-symmetric cross-sections.

• It was shown that shear deformation effects are influential when predicting the response of short span cantilevers. They were also found to be important when predicting the response under steady state analyses.

• The solution provides excellent agreement with shell finite elements at a fraction of the computational and modeling effort.

• The finite element provides superior response predictions than Abaqus B31OS beam element and Vlasov solution with a significantly smaller number of degrees of freedom.

References

Ambrosini, D. (2004), "On free vibration of nonsymmetrical thin-walled beams", *Thin Wall. Struct.*, **47**(6-7), 629-636.

Back, S.Y. and Will, K.M. (1998), "A shear-flexible element with warping for thin-walled open beams", *Int. J. Numer. Meth. Eng.*, **43**(7), 1173-1191.

Banerjee, J.R., Guo, S. and Howson, W.P. (1996), "Exact dynamic stiffness matrix of a bending-torsion coupled beam including warping", *Comput. Struct.*, **59**(4), 613-621.

Bishop, R.E., Cannon, S. and Miao, S. (1989), "On coupled bending and torsional vibration of uniform beams", *J. Sound Vib.*, **131**(3), 457-464.

Bishop, R.E. and Price, W.G. (1985), "A note on the dynamical behavior of uniform beams having open channel section", *J. Sound Vib.*, **99**(2), 155-167.

Chen, X. and Tamma, K. (1994), "Dynamic response of elastic thin-walled structures influenced by coupling effects", *Comput. Struct.*, **51**(1), 91-105.

Chen, W.F. and Lui, E.M. (1997), *Handbook of Structural Engineering*, CRC Press, New York, USA.

Cortinez, V.H. and Piovan, M.T. (2001), "Vibration and buckling of composite thin-walled beams with shear deformability", *J. Sound Vib.*, **258**(4), 701-723.

De Bordon, F. and Ambrosini, D. (2010), "On free vibration analysis of thin-walled beams axially loaded", *Thin Wall. Struct.*, **48**(12), 915-920.

Dokumaci, E. (1987), "An exact solution for coupled flexural and torsional vibrations of uniform beams having single cross-sectional symmetry", *J. Sound Vib.*, **119**(3), 443-449.

Friberg, P.O. (1985), "Beam element matrices derived from Vlasov's theory of open thin-walled elastic beams", *Int. J. Numer. Meth. Eng.*, **21**(7), 1205-1228.

Giunta, G., Belouettar, S., Biscani, F. and Carrera, E. (2014), "Hierarchical theories for a linearised stability analysis of thin-walled beams with open and closed cross-section", *Adv. Aircraft Spacecraft Sci.*, **1**(3), 253-271

Hashemi, S.M. and Richard, M.J. (2000a), "A dynamic finite element method for free vibrations of bending-

torsion coupled beams", *Aerosp. Sci. Tech.*, **4**(1), 41-55.
Hashemi, S.M. and Richard, M.J. (2000b), "Free vibrational analysis of axially loaded bending-torsion coupled beams - a dynamic finite element", *Comput. Struct.*, **77**(6), 711-724.
Hjaji, M.A. and Mohareb, M. (2011a), "Steady state response of doubly symmetric thin-walled members under harmonic excitations - Closed-form solution", *Second International Engineering Mechanics and Materials Specialty Conference*, Ottawa, Canada, June.
Hjaji, M.A. and Mohareb, M. (2011b), "Steady state response of doubly symmetric thin-walled members under harmonic excitations - Finite element formulation", *Second International Engineering Mechanics and Materials Specialty Conference*, Ottawa, Canada, June.
Hjaji, M.A. and Mohareb, M. (2013a), "Harmonic response of doubly symmetric thin-walled members based on the Vlasov theory- I. Analytical solution", *3rd Specialty Conference on Material Engineering & Applied Mechanics*, Montreal, Canada, May.
Hjaji, M.A. and Mohareb, M. (2013b), "Harmonic response of doubly symmetric thin-walled members based on the Vlasov theory - II. Finite element formulation", *3rd Specialty Conference on Material Engineering & Applied Mechanics*, Montreal, Canada, May.
Hjaji, M.A. and Mohareb, M. (2014a), "Coupled flexural-torsional response of harmonically excited mono-symmetric thin-walled Vlasov beams - II. Finite element solution", *4th International Structural Specialty Conference*, Halifax, Nova Scotia, Canada, May
Hjaji, M.A. and Mohareb, M**.** (2014b), "Coupled flexural-torsional response of harmonically excited mono-symmetric thin-walled Vlasov beams - I. Closed form solution", *4th International Structural Specialty Conference*, Halifax, Nova Scotia, Canada, May.
Hu, Y., Jin, X. and Chen, B. (1996), "A finite element model for static and dynamic analysis of thin-walled beams with asymmetric cross-sections", *Comput. Struct.*, **61**(5), 897-908.
Kim, M.Y., Kim, N. and Yun, H.T. (2003), "Exact dynamic and static stiffness matrices of shear deformable thin-walled beam-columns", *J. Sound Vib.*, **267**(1), 29-55.
Kim, N.I. and Kim, M.N. (2005), "Exact dynamic/static stiffness matrices of non-symmetric thin-walled beams considering coupled shear deformation effects", *Thin Wall. Struct.*, **43**(5), 701-734.
Kim, N., Chung, C.F. and Kim, M.Y. (2007), "Stiffness matrices for flexural-torsional/lateral buckling and vibration analysis of thin-walled beam", *J. Sound Vib.*, **299**(4-5), 739-756.
Kollar, J.P. (2001), "Flexural-torsional vibration of open section composite columns with shear deformation", *Int. J. Solid. Struct.*, **38**(42-43), 7543-7558.
Laudiero, F. and Savoia, M. (1991), The shear strain influence on the dynamics of thin-walled beams", *Thin Wall. Struct.*, **11**(5), 375-407.
Leung, A.Y.T. (1991), "Natural shape functions of a compressed Vlasov element", *Thin Wall. Struct.*, **11**(5), 431-438.
Lee, J. and Kim, S.E. (2002a), "Free vibration of thin-walled composite beams with I-shaped cross-sections", *Comput. Struct.*, **55**(2), 205-215.
Lee, J. and Kim, S.E. (2002b), "Flexural-torsional coupled vibration of thin-walled composite beams with channel sections", *Comput. Struct.*, **80**(2), 133-144.
Librescu, L. and Song, O. (2006), *Thin-Walled Composite Beams - Theory and Application*, Springer, Netherland.
Li, J., Hua, H., Shen, R. and Jin, X. (2004a), "Dynamic response of axially loaded monosymmetrical thin-walled Bernoulli-Euler beams", *Thin Wall. Struct.*, **42**(12), 1689-1707.
Li, J., Shen, R., Hua, H. and Jin, X. (2004b), "Response of monosymmetric thin-walled Timoshenko beams to random excitations", *Int. J. Solid. Struct.*, **41**(22-23), 6023-6040.
Li, J, Shen, R., Hua, N. and Jin, X. (2004c), "Coupled bending and torsional vibration of axially loaded thin-walled Timoshenko beams", *Mech. Int. J. Mech. Sci.*, **46**(2), 299-320.
Machado, S.P. and Cortinez, V.H. (2007), "Free vibration of thin-walled composite beams with static initial stresses and deformations", *Eng. Struct.*, **29**(3), 372-382.
Machado, S.P. (2007), "Geometrically non-linear approximations on stability and free vibration of composite beams", *Eng. Struct.*, **29**(12), 3567-3578.

Mei, C. (1970), "Coupled vibrations of thin-walled beams of open section using the finite element method", *Int. J. Mech. Sci.*, **12**(10), 883-891.
Prokic, A. (2006), "On fivefold coupled vibrations of Timoshenko thin-walled beams", *Eng. Struct.*, **28**(1), 54-62.
Prokic, A., Lukic D. and Ladjinovic, D. (2014), "Automatic analysis of thin-walled laminated composite sections", *Steel Compos. Struct.*, **16**(3), 233-252.
Tanaka, M. and Bercin, A.N. (1997), "Finite element modeling of the coupled bending and torsional free vibration of uniform beams with an arbitrary cross-section", *Appl. Math. Model.*, **21**(6), 339-344.
Tanaka, M. and Bercin, A.N. (1998), "Free vibration solution for uniform beams of nonsymmetrical cross-section using mathematica", *Comput. Struct.*, **71**(1), 1-8.
Vlasov, V. (1961), *Thin-Walled Elastic Beams*, Israel Program for Scientific Translation, Jerusalem.
Voros, G.M. (2008), "On coupled vibrations of beams with lateral loads", *J. Comput. Appl. Mech.*, **9**, 1-14.
Voros, G.M. (2009), "On coupled bending-torsional vibrations of beams with initial loads", *Mech. Res. Commun.*, **36**(5), 603-611.
Vo, T.P. and Lee, J. (2009a), "Free vibration of axially loaded thin-walled composite box beams", *Compos. Struct.*, **90**(2) 233-241.
Vo, T.P. and Lee, J. (2009b), "On six-fold coupled buckling of thin-walled composite beams", *Compos. Struct.*, **90**(3), 295-303.
Vo, T.P. and Lee, J. (2009c), "Flexural-torsional coupled vibration and buckling of thin-walled open section composite beams using shear-deformable beam theory", *Int. J. Mech. Sci.*, **51**(9-10), 631-641.
Vo, T.P., Lee, J. and Ahn, N. (2009), "On sixfold coupled vibrations of thin-walled composite box beams", *Compos. Struct.*, **89**(4), 524-535.
Vo, T.P. and Lee, J. (2010), "Interaction curves for vibration and buckling of thin-walled composite box beams under axial loads and end moments", *Appl. Math. Model.*, **34**, 3142-3157.
Vo, T.P., Lee, J. and Lee, K. (2010), "On triply coupled vibrations of axially loaded thin-walled composite beams", *Compos. Struct.*, **88**(3-4), 144-153.
Vo, T.P., Lee, J., Lee, K. and Ahn, N. (2011), "Vibration analysis of thin-walled composite beams with I-shaped cross-sections", *Compos. Struct.*, **93**(2), 812-820.
Wu, L. and Mohareb, M. (2011), "Buckling of shear deformable thin-walled members - I. variational principle and analytical solutions", *Thin Wall. Struct.*, **49**(1), 197-207.

CC

Symbols

A	Cross-sectional area
b	Flange width
C	Centroid of the cross-section
C_w	Warping constant
d	Cross-section height
D_{xx}, D_{yy}, D_{hy}, $D_{\omega\omega}$	Section properties defined by Eq. (16)
E	Modulus of elasticity
G	Shear modulus
$h(s)$	Normal distance between the shear centre and the tangent to mid-surface
H	Beam cross-section height the flanges mid-surfaces
I_{xx}, I_{yy}	Moment of inertias of the cross-section about the principal X and Y axes
J	St. Venant torsional constant

ℓ	Length of the member
$m_j(z,t)$	Distributed harmonic moments about j-th direction (for $j=x,y,z$)
$m_w(z,t)$	Distributed harmonic bimoment
n,s,z	Local curvilinear coordinate system
N_z	Concentrated end forces along longitudinal axis
$q_j(z,t)$	Distributed harmonic forces along x,y,z directions (for $j=x,y,z$)
$r(s)$	Distance between the shear centre to the point of interest along the tangential direction
s	Curvilinear coordinate along mid-surface of the section
S_c	Shear centre of the cross-section
t	Time in seconds
t_1, t_2	Time intervals
T^*	Kinetic energy
u,v	Displacements of the shear centre along the principal axes X, Y
u_p, v_p	Displacements of a point p on the mid-surface of the section along X, Y, Z axes
U^*	Internal strain energy
$V_j(z,t)$	Shear forces along x,y axes (for $j=x,y$)
w	Average longitudinal displacement of the cross-section
W^*	Work done by applied forces
x,y,z	Cartesian coordinate system
X, Y, Z	Principal coordinate system
$x(s)$, $y(s)$	Coordinate of arbitrary point on mid-surface of the section along X and Y axes
x_s	Coordinate of the shear centre along the axis of symmetry
z	Longitudinal coordinate
ε_{zz}	Longitudinal normal strain
γ_{zs}	Shear strain at the mid-surface of the cross-section
ρ	Density of the material
r_0	Polar radius of gyration about the shear centre
ξ, η	Tangential and normal displacements of a point p along s and n directions
θ_x, θ_y, θ_z	Rotations angles around the X, Y, Z axes, respectively
$\hat{\alpha}(s)$	Angle between the tangent to the cross-section and the principal X axis
ψ	Warping deformation function
Ω	Exciting frequency
$\omega(s)$	Warping function of the cross-section

Appendix A. Coefficients of the characteristic polynomial

The characteristic equation based on the expansion of the determinant of Eq. (19) takes the form $B_4 m_i^8 + B_3 m_i^6 + B_2 m_i^4 + B_1 m_i^2 + B_0 = 0$ in which

$$B_4 = E^2 I_{xx} C_w G^2 \left[D_{yy}\left(J + D_{\omega\omega}\right) - D_{hy}^2 \right],$$

$$\begin{aligned} B_3 = \Big[& G\left(J + D_{\omega\omega}\right)\left\{ EI_{xx} GD_{yy}\left(\rho C_w \Omega^2 - GD_{\omega\omega}\right) + EI_{xx} G^2 D_{hy}^2 \right\} + EG^3 D_{yy}\left(I_{xx} D_{\omega\omega}^2 + C_w D_{hy}^2\right) \\ & + \rho\Omega^2 EI_{xx} C_w \left\{ EAG\left(r_o^2 D_{yy} + 2x_s D_{hy}\right) + \left(GD_{yy} + EA\right) \right\} \\ & - EG^2 D_{hy}^2 \left\{ G\left(D_{\omega\omega} I_{xx} - C_w D_{yy}\right) + 2\rho I_{xx} C_w \Omega^2 \right\} \Big] \end{aligned},$$

$$\begin{aligned} B_2 = GD_{yy} \Big[& \left(\rho C_w \Omega^2 - GD_{\omega\omega}\right)\left\{ \rho A\Omega^2 r_o^2 EI_{xx} + G\left(J + D_{\omega\omega}\right)\left(\rho I_{xx}\Omega^2 - GD_{yy}\right) \right. \\ & \left. + G^2\left(D_{yy} J + D_{yy} D_{\omega\omega}\right) - \rho I_{xx}\Omega^2\left(D_{hy}/D_{yy}\right)\left(GD_{hy} - 2EAx_s\right) \right\} \\ & + \left(\rho I_{xx}\Omega^2 - GD_{yy}\right)\left\{ \rho A\Omega^2 r_o^2 EC_w + G^2 D_{\omega\omega}^2 \right\} + G^3 D_{hy}^2\left(D_{\omega\omega} - J\right) \Big] \\ & + \left(\rho I_{xx}\Omega^2 - GD_{yy}\right)\left[G^3 D_{hy}^2\left(J - D_{\omega\omega}\right) + 2\rho A\Omega^2 x_s EC_w GD_{hy} \right] \\ & + \rho A\Omega^2 \Big[G\left(J + D_{\omega\omega}\right)\left\{ EI_{xx}\left(\rho C_w \Omega^2 - GD_{\omega\omega}\right) + EC_w\left(\rho I_{xx}\Omega^2 - GD_{yy}\right) \right\} \\ & + EG^2\left\{ I_{xx} D_{\omega\omega}^2 + C_w D_{hy}^2 \right\} + \rho A\Omega^2 E^2 I_{xx} C_w \left(r_o^2 - x_s^2\right) \\ & + EG^2 r_o^2\left(I_{xx} D_{hy}^2 + C_w D_{yy}^2\right) + 2x_s EG^2 D_{hy}\left(C_w D_{yy} + I_{xx} D_{\omega\omega}\right) \Big] \\ & + G^2 D_{yy}\left[G^2 D_{yy} D_{\omega\omega}^2 + 2D_{hy}^2\left(G^2\left\{J - D_{\omega\omega}\right\} - EC_w\right) \right] \end{aligned},$$

$$\begin{aligned} B_1 = \rho A\Omega^2 \Big[& GD_{yy} r_o^2 \left\{ \left(\rho I_{xx}\Omega^2 - GD_{yy}\right)\left(\rho C_w \Omega^2 - GD_{\omega\omega}\right) - G^2 D_{hy}^2 \right\} \\ & + G^2 D_{hy}\left\{ 2x_s\left(GD_{yy} D_{\omega\omega} + D_{hy}\right) + 2GD_{hy}\left(r_o^2 D_{yy} - x_s D_{hy}\right) \right\} \\ & + \Big[\left(\rho C_w \Omega^2 - GD_{\omega\omega}\right)\left\{ \rho A\Omega^2 EI_{xx}\left(r_o^2 - x_s^2\right) + G\left(J + D_{\omega\omega}\right)\left(\rho I_{xx}\Omega^2 - GD_{yy}\right) \right. \\ & \left. + G^2 D_{hy}^2\left(r_o^2 + 1\right) + 2x_s G^2 D_{yy} D_{hy} \right\} + \left(\rho I_{xx}\Omega^2 - GD_{yy}\right)\left\{ \rho A\Omega^2 r_o^2 EC_w + G^2 D_{\omega\omega}^2 \right\} \\ & + G^3 D_{hy}^2\left(D_{\omega\omega} - J\right) + \left(\rho I_{xx}\Omega^2 - GD_{yy}\right)\left\{ r_o^2 G^2 D_{hy}^2 + \rho\Omega^2 C_w x_s\left(2GD_{hy} - EAx_s\right) \right\} \Big] \Big] \end{aligned},$$

and

$$B_o = \left(\rho A\Omega^2\right)^2\left(r_o^2 - x_s^2\right)\left[\left(\rho I_{xx}\Omega^2 - GD_{yy}\right)\left(\rho C_w \Omega^2 - GD_{\omega\omega}\right) - G^2 D_{hy}^2 \right]$$

Appendix B. Integration constants for cantilever under uniform member loads and tip loads

A cantilever is subjected to (i) uniformly distributed generalized harmonic forces: lateral force $q_y(z,t)=\overline{q}_y\, e^{i\Omega t}$, distributed moments about the axis of symmetry $m_x(z,t)=\overline{m}_x\, e^{i\Omega t}$, twisting moments $m_z(z,t)=\overline{m}_z\, e^{i\Omega t}$ and bimoments $m_w(z,t)=\overline{m}_w\, e^{i\Omega t}$, and (ii) concentrated harmonic forces acting at the tip consisting of a lateral force $P_y(\ell,t)=\overline{P}_y(\ell)e^{i\Omega t}$, bending moment $M_x(\ell,t)=\overline{M}_x(\ell)e^{i\Omega t}$, concentrated torque $M_z(\ell,t)=\overline{M}_z(\ell)e^{i\Omega t}$ and concentrated bimoment $M_w(\ell,t)=\overline{M}_w(\ell)e^{i\Omega t}$. It is required to determine the integration constants $\{\overline{B}\}_{8\times1}$ for the problem.

At the fixed end (i.e., z=0), the boundary conditions are $\overline{v}(0)=\overline{\theta}_x(0)=\overline{\theta}_z(0)=\overline{\psi}(0)=0$ which are expressed in a matrix form as

$$\left[\overline{G}\right]_{4\times8}\left\{\overline{B}\right\}_{8\times1}=-\left\{\overline{U}_{3P}\right\}_{4\times1} \tag{B.1}$$

Also, at the free end $z=\ell$, the natural boundary conditions are

$$\left[\begin{bmatrix} GD_{yy}\mathcal{D} & GD_{yy} & GD_{hy}\mathcal{D} & GD_{hy} \\ 0 & EI_{xx}\mathcal{D} & 0 & 0 \\ GD_{hy}\mathcal{D} & GD_{hy} & \left(GD_{ww}+GJ\right)\mathcal{D} & GD_{\omega\omega} \\ 0 & 0 & 0 & EC_w\mathcal{D} \end{bmatrix}\begin{Bmatrix} \overline{v}(z) \\ \overline{\theta}_x(z) \\ \overline{\theta}_z(z) \\ \overline{\psi}(z) \end{Bmatrix}\right]_{\ell}=\begin{Bmatrix} \overline{V}_y(\ell) \\ \overline{M}_x(\ell) \\ \overline{M}_z(\ell) \\ \overline{M}_w(\ell) \end{Bmatrix} \tag{B.2}$$

which can be shown to lead to the matrix identity

$$\left[\overline{P}\right]_{4\times8}\left\{\overline{B}\right\}_{8\times1}=\left\{\overline{F}(\ell)\right\}_{4\times1} \tag{B.3}$$

in which

$$\left[\overline{P}\right]_{4\times8}=\left[\{p_1\}\ \{p_2\}\ \cdots\cdots\ \{p_8\}\right],$$

$$\{p_i\}=\begin{Bmatrix} \overline{G}_{1,1}GD_{yy}m_i+\overline{G}_{2,1}GD_{yy}+\overline{G}_{3,1}GD_{hy}+GD_{hy} \\ \overline{G}_{2,1}EI_{xx}m_i \\ \overline{G}_{1,1}GD_{hy}m_i+\overline{G}_{2,1}GD_{hy}+\overline{G}_{3,1}\left(GD_{ww}+GJ\right)m_i+GD_{\omega\omega} \\ EC_w m_i \end{Bmatrix}e^{m_i\ell},\ \text{and}\ \left\{\overline{F}(\ell)\right\}_{4\times1}=\begin{Bmatrix} \overline{V}_y(\ell) \\ \overline{M}_x(\ell) \\ \overline{M}_z(\ell) \\ \overline{M}_w(\ell) \end{Bmatrix}.$$

By consolidating Eqs. (B.1) and (B.3) into a single matrix equation and solving for $\{\overline{B}\}_{8\times1}$, one obtains

$$\left\{\overline{B}\right\}_{8\times1}=\begin{bmatrix}\left[\overline{G}\right]_{4\times8} \\ \left[\overline{P}\right]_{4\times8}\end{bmatrix}^{-1}\begin{Bmatrix}-\left\{\overline{U}_{3P}\right\}_{4\times1} \\ \left\{\overline{F}(\ell)\right\}_{4\times1}\end{Bmatrix} \tag{B.4}$$